Fuel 254 (2019) 115641

Contents lists available at ScienceDirect

Fuel

journal homepage: www.elsevier.com/locate/fuel

Full Length Article

Immobilization of elemental mercury in non-ferrous metal smelting gas using $ZnSe_{1-x}S_x$ nanoparticles

Wei Liu[a], Haomiao Xu[a,*], Yongfu Guo[b], Yong Yuan[a], Yong Liao[a], Zan Qu[a], Naiqiang Yan[a]

[a] School of Environmental Science and Engineering, Shanghai Jiao Tong University, Shanghai 200240, China
[b] Suzhou University of Science and Technology, Suzhou 215009, China

GRAPHICAL ABSTRACT

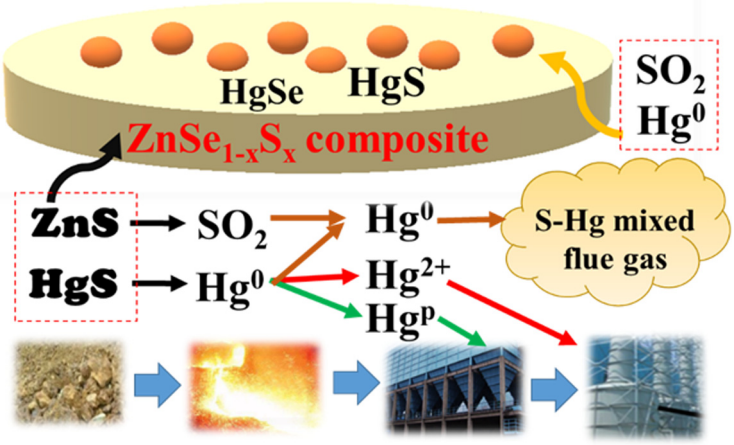

ARTICLE INFO

Keywords:
Elemental mercury
Selenium
Zinc sulfide
Non-ferrous smelting gas
Sulfur dioxide

ABSTRACT

Gaseous elemental mercury (Hg^0) in non-ferrous smelting gas is generally accompanied by a high concentration of SO_2. Traditional sorbents for Hg^0 removal often suffer from SO_2 poisoning. To develop a sorbent that has high mercury removal efficiency and excellent sulfur resistance, Zn-Se-S composites were selected. The experimental results indicated that the $ZnSe_{0.7}S_{0.3}$ composite had the best Hg^0 removal performance, achieving an Hg^0 removal efficiency higher than 99% after 120 min of reaction at 150 °C. A "hump" was observed in the adsorption breakthrough curve. This phenomenon is due to the activation of surface Se^0, with reduction in surface oxidation state (from Se^{2+} to Se^0) by Hg^0 or SO_2. This composite has multiple adsorption sites (Se^0 and active S) for mercury uptake from smelting gas. Moreover, this specific Zn-Se-S composite had excellent SO_2 resistance. Even high concentrations (1000 or 2000 ppm) of SO_2 barely influenced Hg^0 removal performances. The Zn-Se-S composite exhibited potential for Hg^0 removal from non-ferrous smelting gas.

* Corresponding author.
E-mail address: xuhaomiao@sjtu.edu.cn (H. Xu).

https://doi.org/10.1016/j.fuel.2019.115641
Received 22 March 2019; Received in revised form 27 May 2019; Accepted 11 June 2019
Available online 15 June 2019

1. Introduction

Mercury is a hazardous element in the environment owing to its high toxicity, long persistence, and bioaccumulation ability [1,2]. The ***Minamata Convention on Mercury***, a global treaty aimed at controlling mercury from primary emission sources and replacing mercury products such as mercurial thermometers and fluorescent lamps, was approved by 128 countries on August 16, 2017 [3]. China has always been considered the country with the highest mercury emissions. Mercury emissions from coal-fired power plants and non-ferrous metal smelting plants are two primary anthropogenic sources [4–6]. Nowadays, most of the mercury emitted from coal-fired power plants can be efficiently captured using current devices, such as electrostatic precipitators/fabric filter precipitators (ESP/FF), selective catalytic reduction (SCR) units, and wet flue gas desulfurization (WFGD) equipment [7–9]. However, there are no suitable technologies for mercury removal from non-ferrous smelting gas.

Among various non-ferrous metal smelting processes, zinc production is a typical one [10–12]. The general process for Zn production and waste disposal is illustrated in Fig. S1. Hg and Zn elements are sulfophile elements and often exist as HgS and ZnS, respectively, in ores. After smelting in the roaster, mercury will be emitted from the ores at high temperature and exist as gaseous elemental mercury (Hg^0) in the smelting gas. In addition, the associated sulfur in ores will be converted to SO_2. High concentrations of SO_2 and Hg^0 coexist in the smelting gas, forming S-Hg mixed smelting gas. In general, mercury and SO_2 in the smelting gas can get the level of 10 mg·m^{-3} and 4–5%, respectively [13,14]. High concentration of SO_2 is used to produce sulfuric acid (H_2SO_4) after purification system. With decreasing temperature, part of the Hg^0 can transform to oxidized mercury (Hg^{2+}) via reaction with some oxidative components. Part of the Hg^0 will be converted to small particulate mercury (Hg^p) in the smelting gas. Hg^p can be captured in dust removal devices. Hg^{2+} can be captured by scrubbers due to its solubility, and dissolved Hg^{2+} in washing liquid could result in the generation of waste acid that contains mercury. It is difficult to dispose of such wastewater. However, it cannot be efficiently captured using scrubbing towers owing to the high volatility and insolubility of Hg^0. According to our test results at the zinc smelter, the Hg^0 removal efficiency of the scrubbing process and electrostatic demister is 18% and 48%, respectively. This part of mercury also flows into the waste acid. Besides, Hg^0 will enter the acid production process, which would affect the quality of H_2SO_4 product. Moreover, Hg^0 will be eventually emitted from the tail gas into the atmosphere. Therefore, an efficient method for mercury control is the removal of Hg^0 upstream of scrubbing towers. Developing novel sorbents for Hg^0 capture is the key. It is noteworthy that high concentrations of SO_2 coexist with Hg^0 in smelting gas.

Various traditional sorbents have been developed for mercury capture. Carbon-based materials, metal oxides, and some noble metals are widely reported materials for mercury removal [7,15–17]. Carbon-based materials, such as active carbon (AC), are widely used for Hg^0 removal owing to its abundant porous structure. AC injection technology is often used in coal-fired power plants. However, pure AC sorbent has low mercury adsorption capacity owing to its physical adsorption mechanism. Some modified carbon-based materials, such as sulfur- and halogen-modified AC, can enhance mercury adsorption capacities [18–20]. The adsorption capacities of such materials are much higher than those of many kinds of traditional metal oxides, such as iron oxides (FeO_x), manganese oxides (MnO_x), and cobalt oxides (CoO_x) [21–23]. MnO_x is regarded as the most efficient Hg^0 sorbent because of its high affinity for mercury [24–27]. However, Mn-based oxides easily suffer from SO_2 poisoning, especially at high SO_2 concentrations [28,29]. These oxides are not suitable for application in non-ferrous smelting gas. Some noble metals such as Ag and Au have also indicated mercury adsorption performance [30–32]. However, their industrial usage seems unlikely owing to their high price. Therefore, it is necessary to develop novel materials that have excellent SO_2 resistance and high mercury capacity.

Sulfur minerals with abundant reduced sulfur species, which has a strong affinity with mercury. Yang et al. used magnetic pyrrhotite ($Fe_{1-x}S$) to remove Hg^0 [33]. The experimental results indicated that $Fe_{1-x}S$ has a gaseous Hg^0 removal rate of 0.28 μg·(g·min)$^{-1}$ at 60 °C and a Hg^0 adsorption capacity of 0.22 mg·g^{-1}. Li et al. synthesized nano-ZnS particles for Hg^0 removal [34]. The nano-ZnS was superior in both Hg^0 adsorption capacity and reaction rate. Some novel sulfide chalcogels were also selected for gaseous mercury removal [35]. The molybdenum sulfide aerogel exhibited a high adsorption selectivity for iodine and mercury. In our previous studies, it was indicated that $[MoS_4]^{2-}$ clusters could be used for mercury uptake from S-Hg mixed flue gas [36].

Zinc concentrate is the raw material of zinc smelting, and the main ingredient is ZnS. However, pure ZnS has low Hg^0 adsorption capacity. The reason for this could be that ZnS has a stable crystal structure that is not favorable for mercury adsorption on its surface. Selenium and sulfur belong to one chemical family, thus they are alike in nature and have high affinity for each other [37,38]. In addition, Se was shown to be capable of mercury removal [39]. Therefore, we designed a series of $ZnSe_{1-x}S_x$ composites to build a defect structure with high Hg^0 removal efficiency.

In this study, a series of Se-modified ZnS composites were synthesized, and their mercury capture performance were investigated in simulated flue gas. The optimal reaction temperature and the influence of flue gas components on Hg^0 removal efficiency were studied. The Hg^0 removal mechanism was also analyzed based on the experimental and characterization results. The ultimate aim is to develop an effective adsorbent which is suitable for industrial application in Hg^0 removal from non-ferrous smelting flue gas.

2. Experimental section

2.1. Preparation of materials

Preparation of $ZnSe_{1-x}S_x$ nanoparticles: In a typical procedure, $Zn(NO_3)_2$ was first dissolved in 100 mL of ethanol. Then, Se powder and Na_2S solution were added and the mixture was heated at 100 °C for 2 h. The molar ratio of Zn:(S + Se) was 1:1. Then, the mixture was transferred into a 200 mL Teflon-lined stainless-steel autoclave. The autoclave was sealed and heated at 120 °C for 12 h, followed by cooling to ambient temperature. The obtained product was thoroughly washed with ethanol and filtered several times and to remove the unreacted nitrates. For comparison, pure ZnS and ZnSe were also synthesized using the same method.

2.2. Characterization of materials

The Powder X-ray diffraction (XRD) patterns were determined by a Shimadzu XRD-6100 diffractometer with Cu Kα radiation at room temperature. The data were recorded at a step of 10° min^{-1} in the range of 10–80°. The surface composition was detected by X-ray photoelectron spectroscopy (XPS). The results were recorded with a XPS instrument (Ultra DLD, Shimadzu-Kratos) with Al Kα as the excitation source, and the binding energy was calibrated using the C 1s line at 284.6 eV.

2.3. Measurement of gaseous mercury adsorption performance

To evaluate the Hg^0 removal efficiencies of the as-prepared materials, a lab-scale fixed-bed adsorption system was assembled. A schematic of this process is shown in the Supporting Information (Fig. S1). This evaluation system contained a feed gas system, gaseous Hg^0 generator, quartz reactor, Hg^0 detection system, and tail-gas purification system. In general, O_2, gaseous Hg^0, and SO_2 vapor were distributed using pure N_2. To provide a constant gaseous Hg^0 (about 1.0 mg·m^{-3}), a Hg^0 permeation device was placed in a unchanged temperature (43 °C)

oil bath. The total flow rate was maintained as 500 mL·min^{-1} with a mass flow controller. For each experiment, 25 mg of prepared samples was placed into a quartz tube with an inner diameter of 5 mm. The off-gas coming from reactor passed through an active carbon and $KMnO_4$ solution the exhaust gas cleaning. The reaction temperatures were controlled from 50 to 150 °C by temperature control devices. Before each test, the simulated flue gas contained Hg^0 was firstly bypassed the sorbent bed and passed into the Hg^0 detection system until the inlet Hg^0 concentration was stable. The inlet and outlet Hg^0 concentrations were detected by a cold-vapor atomic absorption spectrometer (CVAAS) mercury detector, which was calibrated via a Lumex RA 915+. The time for each test was 2 h. The Hg^0 removal efficiencies were calculated according to Eq. (1):

$$Hg^0 \text{ removal efficiency} = \frac{Hg^0_{in} - Hg^0_{out}}{Hg^0_{in}} \quad (1)$$

where $Hg_{in}{}^0$ is the inlet concentration of Hg^0, and $Hg_{out}{}^0$ is the outlet concentration of Hg^0.

3. Results and discussion

3.1. Hg^0 removal performance

3.1.1. Hg^0 removal performance of various materials

The Hg^0 removal performance of as-prepared samples is shown in Fig. 1. ZnS, ZnSe, and $ZnSe_{1-x}S_x$ composites (of different ratios) were tested for comparison under 5% O_2 atmosphere at 100 °C. ZnS nanoparticle had high Hg^0 removal performance (Hg^0 removal efficiency of almost 100%) during the first 20 min of the reaction. However, after 100 min of reaction, the Hg^0 removal efficiency dropped sharply, to only approximately 50%. For the ZnSe composite, the initial removal efficiency was much lower than that of ZnS. However, the Hg^0 removal efficiency gradually increased after the first several minutes. The curve exhibited a "hump" shape. The same phenomenon appeared in the curves of the other $ZnSe_{1-x}S_x$ samples, especially $ZnSe_{0.5}S_{0.5}$. Although $ZnSe_{0.5}S_{0.5}$ had the lowest Hg^0 removal efficiency, the Hg^0 removal efficiency gradually increased after the first 5 min. Among the $ZnSe_{1-x}S_x$ samples, $ZnSe_{0.7}S_{0.3}$ had the highest Hg^0 removal efficiency, approximately 85%, which was maintained throughout the reaction. It was speculated that some of this composite's active sites were activated when it reacted with gaseous Hg^0. For comparison, the Hg^0 adsorption capacity of other sorbents reported in the literatures were summarized in Table S2 [34,40–42].

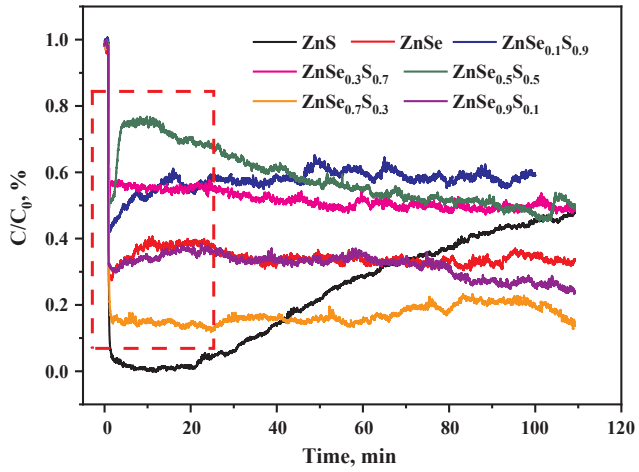

Fig. 1. Hg^0 removal performance of various as-prepared materials 5% O_2 and ~1.0 mg/m^3 Hg^0 with 500 mL/min flow rate, T = 100 °C.

3.1.2. Effect of temperature on Hg^0 removal performance

Temperature is an important factor for gaseous reactions and it determines the applicability of different sorbents for treatment of real smelting gas. In a typical non-ferrous smelting plant, the flue gas temperature at upstream unit of ESP in a zinc production plant is about 250 °C, and the temperature reduced to 30–100 °C after scrubbing towers. The effects of temperature on Hg^0 removal efficiency by $ZnSe_{0.7}S_{0.3}$ are shown in Fig. 2(a). This reaction exhibited some obvious "hump" curves under various reaction temperatures. When the temperature was lower than 100 °C, the final Hg^0 removal efficiencies were approximately 80%. At a temperature of 100 °C, the Hg^0 removal efficiency was about 90% after 120 min of reaction. As the reaction temperature increased, the Hg^0 removal efficiencies further increased. When the reaction temperature was 125 °C, the Hg^0 removal efficiency was nearly 100%. The same phenomenon (higher Hg^0 removal efficiency) was observed at 150 °C. When the temperature was higher than 150 °C, the Hg^0 removal efficiencies were higher than that of low temperatures (< 150 °C). However, the composite was decomposed when the temperature was higher than 150 °C. As shown in Fig. 2(b), the red part at the end of the reaction tube indicates the decomposition products of Se^0. The Zn-Se-S composite was destroyed at such high temperatures [39]. Therefore, the Zn-Se-S composite can only be used at lower temperatures below 150 °C. Moreover, capturing Hg^0 at this temperature can avoid gaseous Hg^0 entering the scrubber system and producing waste acid, which is more difficult to treat.

3.1.3. Effect of SO_2 on Hg^0 removal performance

Obviously, Zn-Se-S composites can be applied at lower temperatures. They can be used upstream of scrubbing towers in a zinc production plant. In this unit, SO_2 was the primary gas component and could reach thousands-ppm level. Usually, SO_2 has a poisonous effect on Hg^0 removal for various kinds of sorbents [20,43]. The effects of SO_2 on Hg^0 removal by $ZnSe_{0.7}S_{0.3}$ were investigated, and the results are shown in Fig. 3(a). The total Hg^0 removal efficiencies were calculated based on the 120 min reaction. When 1000 ppm SO_2 was added to the simulated smelting gas, the Hg^0 removal efficiencies were higher than 90%, whether at 75 °C, 100 °C, or 125 °C. Similarly, when 2000 ppm SO_2 was added to the simulated gas, SO_2 barely influenced Hg^0 removal efficiencies. To further investigate the effect of SO_2, the $ZnSe_{0.7}S_{0.3}$ composite was first pretreated with 1000 ppm or 2000 ppm SO_2 for 2 h. Then, the composites were tested for Hg^0 removal at 100 °C. The results are shown in Fig. 3(b). The Hg^0 removal efficiencies of the pre-sulfurized composites were higher than 90%, even in the first several minutes. These results further indicated that this composite has excellent resistance to SO_2.

3.2. Hg^0 removal mechanism of the Zn-Se-S composite

3.2.1. Physical structure characterization

The X-ray diffraction patterns of the $ZnSe_{1-x}S_x$ samples are presented in Fig. 4. For ZnSe, all diffraction peaks in the XRD patterns belong to crystalline ZnSe and no diffraction peaks of elemental Zn, Se, and S or other components were observed [44]. For ZnS, the XRD peaks corresponded to the standard values for ZnS [45]. For the composites of Zn-Se-S, Se-rich samples mainly presented the structure of ZnSe, whereas S-rich samples primarily presented the structure of ZnS. For $ZnSe_{0.5}S_{0.5}$, it is obvious that the crystal structures of ZnSe and ZnS coexisted. Furthermore, with the addition of Se to ZnS, a porous structure and larger surface area were the results.

3.2.2. Surface chemical analysis

To further investigate the surface composition before and after the reaction, XPS analysis was performed. The spectra for XPS analysis are shown in Fig. 5, and the analysis data are shown in Table S1. As shown in Fig. 5(a), for ZnS, the two peaks centered at 162.9 and 161.7 eV were assigned to surface active sulfur and S^{2-}, respectively [36]. For the

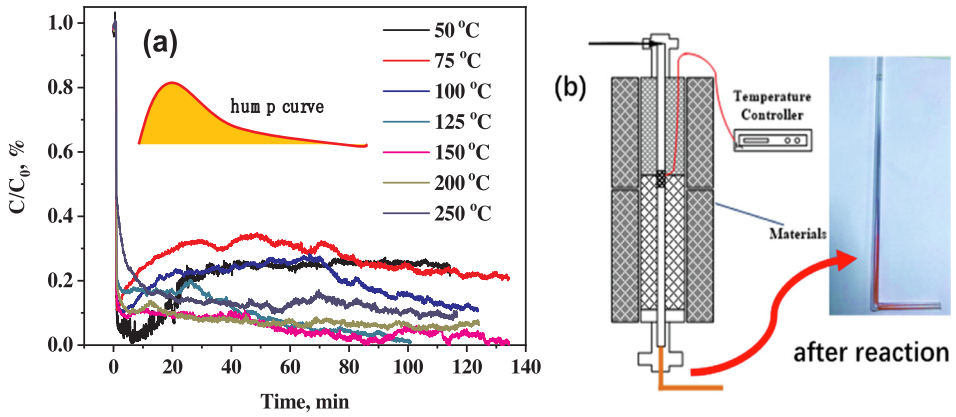

Fig. 2. (a) Effect of temperature on Hg^0 removal performance of the $ZnSe_{0.7}S_{0.3}$ mixed composite and (b) the reaction tube after the reaction at 150 °C 5% O_2 and ~1.0 mg/m^3 Hg^0 with 500 mL/min flow rate.

$ZnSe_{0.7}S_{0.3}$ composite sample, two peaks at 163.1 and 161.8 eV were also assigned to active S and S^{2-}, respectively [34,46]. However, the constitution of these two sulfur species varied. Active S represented 45.35% and 17.48% of the sulfur in ZnS and the $ZnSe_{0.7}S_{0.3}$ composite, respectively. The Se 3d spectra are shown in Fig. 5(b). For ZnSe, the spin orbit splitting of the 3d states was divided into 3d 5/2 and 3d 3/2 states. The observed binding energy of Se 3d 5/2 and Se 3d 3/2 was at 55.1 and 56.0 eV, respectively, which was attributed to Se. For the $ZnSe_{0.7}S_{0.3}$ composite, the peak at 55.3 eV was associated with Se^0 and the broad peak near 58.9 eV indicated the surface oxidation state of Se [47]. Furthermore, the peak at 54.4 eV was assigned to ZnSe in the composite.

After the reaction, the spent composites were also analyzed. As shown in Fig. 5(c), after reaction with Hg^0, for S 2p, two peaks, at 163.2 and 161.9 eV, were assigned to active S and S^{2-}, respectively. However, the ratio of active S to the total sulfur changed after the reaction, increasing from 17.48% of the fresh sample to 21.30% of the spent sample. After the reaction of SO_2 + Hg^0, the peaks' positions were the same as those for the fresh sample. The proportion of active S was further increased to 24.17%. During the reaction, the active S increased on the surface of the composite. As shown in Fig. 5(d), for Se 3d, after reaction with Hg^0, only two peaks, at 59.3 and 54.8 eV, were detected. The peak at 59.3 eV was assigned to the surface oxidation states of Se. And a wide peak was generated from 52–57 eV, indicating that part of high valence of Se was reduced to the low valence state. In addition, part of Se can combine with the Hg^0 and form HgSe after adsorption. Se^{2-} can also combine with Hg^{2+} and form HgSe. It is difficult to distinguish these different binding peak due to the similar binding energies. Therefore, we only can see a wide peak based on the XPS results. The same phenomenon can be seen in the spectrum after the reaction of SO_2 + Hg^0, where only two peaks appeared, which are assigned to the surface oxidation states of Se and the low valence state of Se. In addition, the ratio of Se oxidation state to the total Se dropped from 34.96% in the after Hg^0 reaction sample to 29.07%. This could be the result of the reduction effect of SO_2. Obviously, Se changed significantly during the reaction with Hg^0. Moreover, for the spectra of Hg 4f, as shown in Fig. 5(e), when reacted with Hg^0, two peaks, at 104 and 100.0 eV, were assigned to Hg 4f 5/2 and Hg 4f 7/2, respectively [34,46].

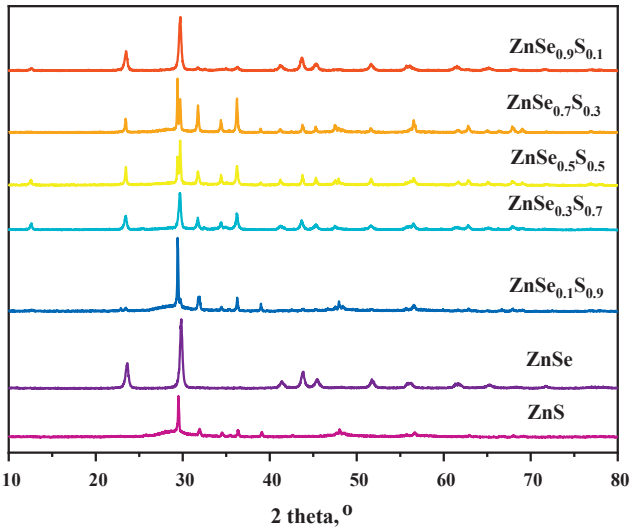

Fig. 4. XRD patterns of the as-prepared $ZnSe_{1-x}S_x$ samples.

Based on the above discussion and as shown in Fig. 6, the Hg^0 removal mechanism can be described as follows. First, gaseous Hg^0 was adsorbed onto the surface of the composite, the larger surface area of

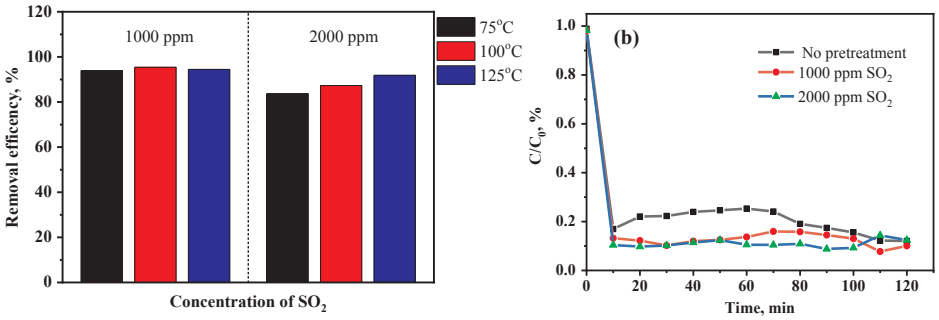

Fig. 3. (a) Effect of SO_2 on Hg^0 removal performance at various reaction temperatures and the (b) effect of SO_2 pretreatment on Hg^0 removal by the $ZnSe_{0.7}S_{0.3}$ mixed composite.

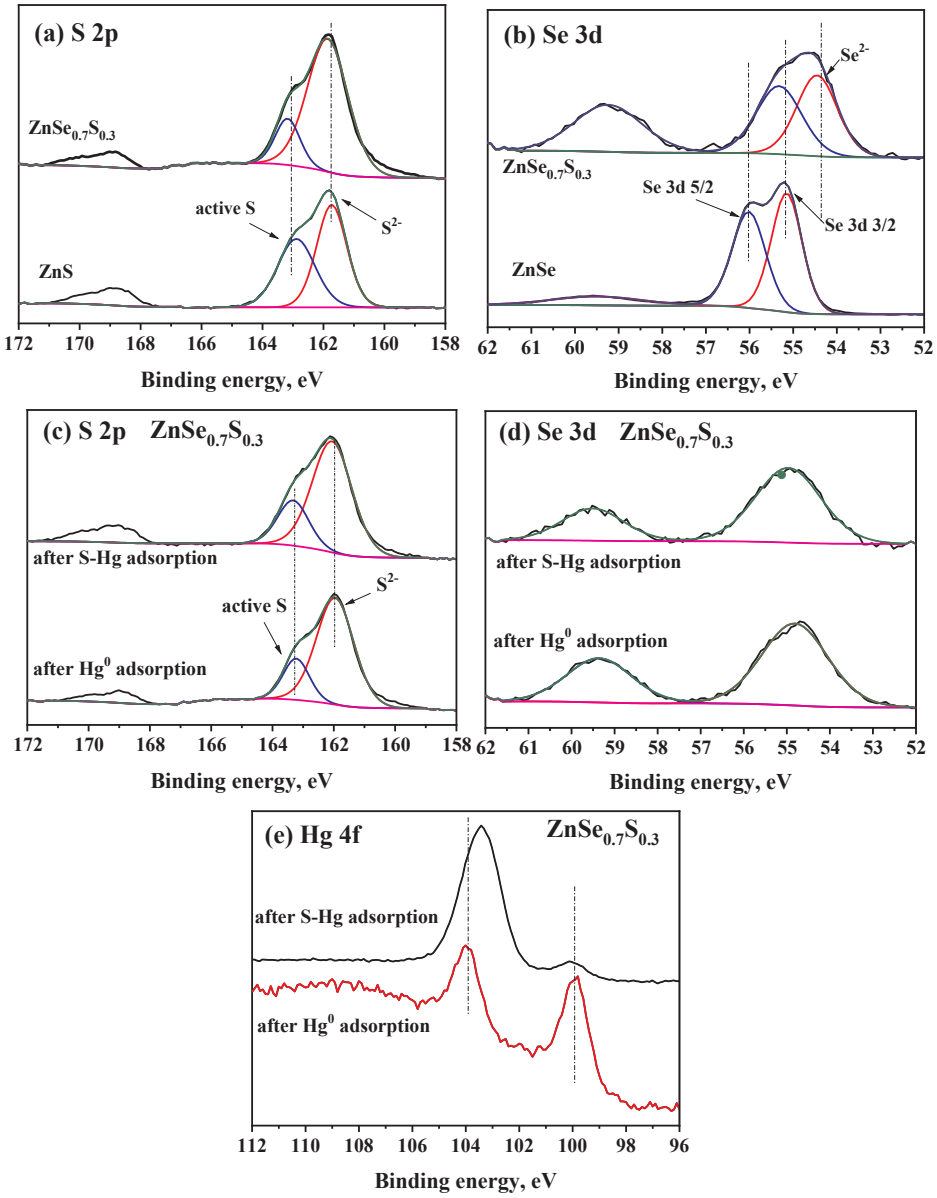

Fig. 5. XPS analysis for (a) S 2p, fresh sample; (b) Se 3d, fresh sample; (c) S 2p, after reaction; (d) Se 3d, after reaction; and (e) Hg 4f, after reaction.

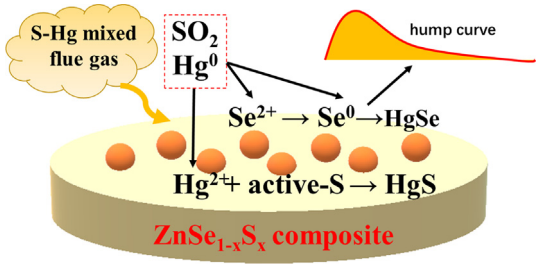

Fig. 6. Proposed removal mechanism of Hg^0 from S-Hg mixed flue gas by Zn-Se-S composites.

which benefits this physical adsorption process, thus adsorbed mercury ($\equiv Hg^0$) was formed. Second, the $\equiv Hg^0$ reacted with Se ($\equiv Se^{2+}$) and transformed to $\equiv Hg^{2+}$ along with the reduction of $\equiv Se^{2+}$ to $\equiv Se^0$. The chemistry of mercury and selenium, particularly the readily interactive electron orbitals of elemental selenium, predisposes its binding to elemental mercury with high affinity [48]. Then, the surface $\equiv Hg^0$ reacted with $\equiv Se^0$ and formed $\equiv$Hg-Se. Herein, we can find the "hump effect," which refers to the activation of surface $\equiv Se^0$. In addition, the surface active S ($\equiv$S) which contains S and S^{2-} also reacted with $\equiv$Hg or $\equiv Hg^{2+}$ and formed surface $\equiv$HgS. The reactions illustrating these processes are as follows:

$$Hg^0 \rightarrow \equiv Hg^0 \quad (2)$$

$$\equiv Hg^0 + \equiv Se^{2+} \rightarrow \equiv Hg^{2+} + \equiv Se^0 \quad (3)$$

$$\equiv Se^0 + \equiv Hg^0 \rightarrow \equiv Hg - Se \quad (4)$$

$$\equiv S\ (S^{2-}/S) + \equiv Hg(\equiv Hg^{2+}/\equiv Hg) \rightarrow 2 \equiv HgS \quad (5)$$

Furthermore, this composite had excellent SO_2 resistance. On one hand, pure Se and surface-active S could not react with SO_2, which protected the composite. On the other hand, SO_2 could react with $\equiv Se^{2+}$ to form $\equiv Se^0$, the surface $\equiv Se^0$ can react with $\equiv Hg^0$ and form HgSe.

Therefore, Zn-Se-S exhibited a higher Hg^0 removal efficiency as well as excellent SO_2 resistance. Such composites have two types of active sites for mercury capture. Se^0 can capture surface Hg^0 and form HgSe. Surface active S can capture surface Hg^{2+} and form HgS. In addition,

SO_2 and Hg^0 can promote the transformation of surface Se^{2+} to Se^0, thereby enhancing Hg^0 removal performance. These characteristics make Zn-Se-S composites promising materials for mercury uptake from a S-Hg mixed flue gas.

4. Conclusion

In this work, the Zn-Se-S ternary composites were synthesized to capture Hg^0 from non-ferrous smelting gas. The Zn-Se-S exhibit higher mercury removal efficiency and excellent SO_2 resistance compared with to that of ZnS and ZnSe. And $ZnSe_{0.7}S_{0.3}$ composite had the best Hg^0 capture performance, achieving an Hg^0 removal efficiency higher than 99% after 120 min at 150 °C. A "hump" effect was observed in the adsorption breakthrough curve, which is due to the activation of surface Se^0, with reduction in surface oxidation state (from Se^{2+} to Se^0) by Hg^0 or SO_2. The multiple adsorption sites (Se^0 and active S) attributed to excellent Hg^0 adsorption capacity from smelting gas, where Hg^0 was immobilized as HgS and HgSe on the Zn-Se-S surface. The $ZnSe_{0.7}S_{0.3}$ has best Hg^0 removal efficiency at 150 °C. Moreover, the addition of 1000 or 2000 ppm SO_2 had a slight effect on Hg^0 removal efficiency, indicating an excellent SO_2 resistance. These results demonstrated the Zn-Se-S can be used upstream of scrubbing towers for mercury uptake, indicating promising material for removing Hg^0 from non-ferrous smelting gas.

Acknowledgements

This study was supported by the National Key R&D Program of China (2017YFC0210500) and the National Natural Science Foundation of China (No. 21806105 and No. 51578354). This study was also supported by the National Postdoctoral Program for Innovative Talents (No. BX201700151). We are grateful for the support of China's Postdoctoral Science Fund (No. 2017M620156).

Appendix A. Supplementary data

Supplementary data to this article can be found online at https://doi.org/10.1016/j.fuel.2019.115641.

References

[1] Driscoll CT, Mason RP, Chan HM, Jacob DJ, Pirrone N. Mercury as a global pollutant: sources, pathways, and effects. Environ Sci Technol 2013;47(10):4967–83.
[2] Selin NE. Global biogeochemical cycling of mercury: a review. Annu Rev Environ Resour 2010;34(1):43–63.
[3] Giang A, Stokes LC, Streets DG, Corbitt ES, Selin NE. Impacts of the minamata convention on mercury emissions and global deposition from coal-fired power generation in Asia. Environ Sci Technol 2015;49(9):5326–35.
[4] Zhang L, Wang S, Wang L, Wu Y, Duan L, Wu Q, et al. Updated emission inventories for speciated atmospheric mercury from anthropogenic sources in China. Environ Sci Technol 2015;49(5):3185–94.
[5] De SF, Gencarelli CN, Hedgecock IM, Pirrone N. A modeling comparison of mercury deposition from current anthropogenic mercury emission inventories. Environ Sci Technol 2016;50(10).
[6] Streets DG, Hao J, Wu Y, Jiang J, Chan M, Tian H, et al. Anthropogenic mercury emissions in China. Atmos Environ 2005;39(40):7789–806.
[7] Pavlish JH, Sondreal EA, Mann MD, Olson ES, Galbreath KC, Laudal DL, et al. Status review of mercury control options for coal-fired power plants. Fuel Process Technol 2003;82(2–3):89–165.
[8] Galbreath KC, Zygarlicke CJ. Mercury transformations in coal combustion flue gas. Fuel Process Technol 2000;65(99):289–310.
[9] Wang SX, Zhang L, Li GH, Wu Y, Hao JM, Pirrone N, et al. Mercury emission and speciation of coal-fired power plants in China. Atmos Chem Phys Discuss 2009;10(3):1183–92.
[10] Zhang L, Wang S, Wu Q, Meng Y, Yang H, Wang F, et al. Were mercury emission factors for Chinese non-ferrous metal smelters overestimated? Evidence from onsite measurements in six smelters. Environ Pollut 2012;171(171):109–17.
[11] Ye X, Hu D, Wang H, Chen L, Xie H, Zhang W, et al. Atmospheric mercury emissions from China's primary nonferrous metal (Zn, Pb and Cu) smelting during 1949–2010. Atmos Environ 2015;103(1):331–8.
[12] Li Z, Ma Z, Kuijp TJVD, Yuan Z, Huang L. A review of soil heavy metal pollution from mines in China: pollution and health risk assessment. Sci Total Environ 2014;468–469:843–53.
[13] Wu Q, Wang S, Hui M, Wang F, Zhang L, Duan L, et al. New insight into atmospheric mercury emissions from zinc smelters using mass flow analysis. Environ Sci Technol 2015;49(6):3532–9.
[14] Wu Q, Wang S, Zhang L, Hui M, Wang F, Hao J. Flow analysis of the mercury associated with nonferrous ore concentrates: implications on mercury emissions and recovery in China. Environ Sci Technol 2016;50(4):1796–803.
[15] Gao Y, Zhang Z, Wu J, Duan L, Umar A, Sun L, et al. A critical review on the heterogeneous catalytic oxidation of elemental mercury in flue gases. Environ Sci Technol 2013;47(19):10813–23.
[16] Cao Y, Chen B, Wu J, Cui H, Smith J, Chen C-K, et al. Study of mercury oxidation by a selective catalytic reduction catalyst in a pilot-scale slipstream reactor at a utility boiler burning bituminous coal. Energy Fuels 2007;21(1):145–56.
[17] Xu W, Wang H, Zhu T, Kuang J, Jing P. Mercury removal from coal combustion flue gas by modified fly ash. J Environ Sci 2013;25(2):393–8.
[18] Hu C, Zhou J, He S, Luo Z, Cen K. Effect of chemical activation of an activated carbon using zinc chloride on elemental mercury adsorption. Fuel Process Technol 2009;90(6):812–7.
[19] Tian L, Li C, Li Q, Zeng G, Gao Z, Li S, et al. Removal of elemental mercury by activated carbon impregnated with CeO. Fuel 2009;88(9):1687–91.
[20] Uddin MA, Yamada T, Ochiai R, Sasaoka E, Wu S. Role of SO 2 for elemental mercury removal from coal combustion flue gas by activated carbon. Energy Fuels 2008;22(4):13–9.
[21] Liu Y, Wang Y, Wang H, Wu Z. Catalytic oxidation of gas-phase mercury over Co/TiO catalysts prepared by sol–gel method. Catal Commun 2011;12(14):1291–4.
[22] Shao Y, Li J, Chang H, Peng Y, Deng Y. The outstanding performance of LDH-derived mixed oxide Mn/CoAlOx for Hg0 oxidation. Catal Sci Technol 2015;5(7):3536–44.
[23] Yang S, Guo Y, Yan N, Wu D, He H, Xie J, et al. Remarkable effect of the incorporation of titanium on the catalytic activity and SO2 poisoning resistance of magnetic Mn–Fe spinel for elemental mercury capture. Appl Catal B 2011;101(3–4):698–708.
[24] Xu H, Qu Z, Zong C, Huang W, Quan F, Yan N. MnOx/graphene for the catalytic oxidation and adsorption of elemental mercury. Environ Sci Technol 2015;49(11):6823–30.
[25] Xu H, Yan N, Qu Z, Liu W, Mei J, Huang W, et al. Gaseous heterogeneous catalytic reactions over Mn-based oxides for environmental applications–a critical review. Environ Sci Technol 2017;51(16):8879.
[26] He C, Shen B, Chen J, Cai J. Adsorption and oxidation of elemental mercury over Ce-MnOx/Ti-PILCs. Environ Sci Technol 2014;48(14):7891.
[27] Li J, Chang H, Ma L, Hao J, Yang RT. Low-temperature selective catalytic reduction of NOx with NH3 over metal oxide and zeolite catalysts—a review. Catal Today 2011;175(1):147–56.
[28] Ma Y, Mu B, Yuan D, Zhang H, Xu H. Design of MnO2/CeO2-MnO2 hierarchical binary oxides for elemental mercury removal from coal-fired flue gas. J Hazard Mater 2017;333:186–93.
[29] Ma Y, Mu B, Zhang X, Yuan D, Ma C, Xu H, et al. Graphene enhanced Mn-Ce binary metal oxides for catalytic oxidation and adsorption of elemental mercury from coal-fired flue gas. Chem Eng J 2019;358:1499–506.
[30] Zhao S, Li Z, Qu Z, Yan N, Huang W, Chen W, et al. Co-benefit of Ag and Mo for the catalytic oxidation of elemental mercury. Fuel 2015;158:891–7.
[31] Rodríguezpérez J, Lópezantón MA, Díazsomoano M, García R, Martíneztarazona MR. Development of gold nanoparticle-doped activated carbon sorbent for elemental mercury. Energy Fuels 2011;25(5):2022–7.
[32] Ma Y, Mu B, Zhang X, Xu H, Qu Z, Gao L, et al. Ag-Fe3O4@rGO ternary magnetic adsorbent for gaseous elemental mercury removal from coal-fired flue gas. Fuel 2019;239:579–86.
[33] Yong L, Dong C, Zou S, Xiong S, Xin X, Hao D, et al. Recyclable naturally derived magnetic pyrrhotite for elemental mercury recovery from flue gas. Environ Sci Technol 2016;50(19):10562.
[34] Li H, Zhu L, Wang J, Li L, Shih K. Development of nano-sulfide sorbent for efficient removal of elemental mercury from coal combustion fuel gas. Environ Sci Technol 2016;50(17):9551–7.
[35] Subrahmanyam KS, Malliakas CD, Sarma D, Armatas GS, Wu J, Kanatzidis MG. Ion-exchangeable molybdenum-sulfide porous chalcogel: gas adsorption and capture of iodine and mercury. J Am Chem Soc 2015;137(43):13943.
[36] Xu H, Yuan Y, Liao Y, Xie J, Qu Z, Shangguan W, et al. [MoS4]2- cluster bridges in Co-Fe layered double hydroxides for mercury uptake from S-Hg mixed flue gas. Environ Sci Technol 2017.
[37] Anantharaj S, Ede SR, Sakthikumar K, Karthick K, Mishra S, Kundu S. Recent trends and perspectives in electrochemical water splitting with an emphasis to sulphide, selenide and phosphide catalysts of Fe, Co and Ni: a review. Catalysis 2016;6(12).
[38] Wang JJ, Xue DJ, Guo YG, Hu JS, Wan LJ. Bandgap engineering of monodispersed Cu2–xSySe1–y nanocrystals through chalcogen ratio and crystal structure. J Am Chem Soc 2011;133(46):18558–61.
[39] Lee JY, Yong JK. Hg(0) removal using Se(0)-doped montmorillonite from selenite (IV). Bull Korean Chem Soc 2013;34(12):3767–70.
[40] Li H, Zhu W, Yang J, Zhang M, Zhao J, Qu W. Sulfur abundant S/FeS2 for efficient removal of mercury from coal-fired power plants. Fuel 2018;232:476–84.
[41] Liao Y, Chen D, Zou S, Xiong S, Xiao X, Dang H, et al. Recyclable naturally derived magnetic pyrrhotite for elemental mercury recovery from flue gas. Environ Sci Technol 2016;50(19):10562–9.
[42] Zou S, Liao Y, Xiong S, Huang N, Geng Y, Yang S. H2S-modified Fe-Ti spinel: a recyclable magnetic sorbent for recovering gaseous elemental mercury from flue gas as a co-benefit of wet electrostatic precipitators. Environ Sci Technol 2017;51(6):3426–34.
[43] Yang Shijian, Guo Yongfu, Yan Naiqiang, Qu Zan, Xie Jiangkun, Yang Chen, et al.

Capture of gaseous elemental mercury from flue gas using a magnetic and sulfur poisoning resistant sorbent Mn/γ-Fe2O3 at lower temperatures. J Hazard Mater 2011;186(1):508.
[44] Park S, Kim H, Jin C, Lee C. Synthesis, structure, and photoluminescence properties of ZnSSe alloy nanorods. Curr Appl Phys 2012;12(2):499–503.
[45] Yu L, Chen W, Li D, Wang J, Yu S, He M, et al. Inhibition of photocorrosion and photoactivity enhancement for ZnO via specific hollow ZnO core/ZnS shell structure. Appl Catal B 2015;164:453–61.
[46] Singh N, Patil K, Khanna P. Nano-sized HgSe powder: single-step preparation and characterization. Mater Sci Eng, B 2007;142(1):31–6.
[47] Zhu H, Jiang R, Chen X, Chen Y, Wang L. 3D nickel-cobalt diselenide nanonetwork for highly efficient oxygen evolution. Sci Bull 2017.
[48] Ralston N. Nanomaterials: nano-selenium captures mercury. Nat Nanotechnol 2008;3(9):527.